The geometry of chaos synchronization

Ernest Barreto[a)]
Department of Physics and Astronomy and the Krasnow Institute for Advanced Study, George Mason University, Fairfax, Virginia 22030

Krešimir Josić
Department of Mathematics and Statistics and the Center for BioDynamics, Boston University, Boston, Massachusetts 02215

Carlos J. Morales
Department of Mathematics and Statistics, Boston University, Boston, Massachusetts 02215

Evelyn Sander
Department of Mathematical Sciences, George Mason University, Fairfax, Virginia 22030

Paul So
Department of Physics and Astronomy and the Krasnow Institute for Advanced Study, George Mason University, Fairfax, Virginia 22030

(Received 16 April 2002; accepted 16 August 2002; published 21 February 2003)

Chaos synchronization in coupled systems is often characterized by a map ϕ between the states of the components. In noninvertible systems, or in systems without inherent symmetries, the synchronization set—by which we mean graph(ϕ)—can be extremely complicated. We identify, describe, and give examples of several different complications that can arise, and we link each to inherent properties of the underlying dynamics. In brief, synchronization sets can in general become nondifferentiable, and in the more severe case of noninvertible dynamics, they might even be multivalued. We suggest two different ways to quantify these features, and we discuss possible failures in detecting chaos synchrony using standard continuity-based methods when these features are present. © *2003 American Institute of Physics.* [DOI: 10.1063/1.1512927]

Since the surprising discovery that chaotic systems can synchronize,[1,2] many different kinds of nonlinear synchrony have been considered in the literature.[3] We focus here on the geometry of synchronization structures that arise in such systems and point out several complicating factors that are not generally appreciated. These more complicated states may arise in noninvertible systems, in systems with critical points, and in systems of significantly dissimilar nonlinear elements. An important case is that of neuronal systems, which consist of many very different interacting classes of neurons, each of which exhibit great variation in their morphology. Nontrivial synchronous relationships in such systems may have physiological significance, and may even correspond to perceptual events.[4] We identify several different geometric features that can arise in these more complicated situations, giving several examples and providing an intuitive explanation for each case. A good understanding of these inherent mathematical features is important for the proper interpretation of experimental data, especially in situations in which the detection and classification of such synchronous states is of interest. In particular, we find that most existing methods for detecting synchrony[5–7] will be hampered by the inherent geometric features that we identify.[8]

[a)]Web site: http://complex.gmu.edu

I. INTRODUCTION

In this work we consider a general drive/response system $\mathbf{F}:X\times Y\to X\times Y$, where $(\mathbf{x}_{n+1},\mathbf{y}_{n+1})=\mathbf{F}(\mathbf{x}_n,\mathbf{y}_n)$ and is of the form,

$$\mathbf{x}_{n+1}=\mathbf{f}(\mathbf{x}_n),$$

$$\mathbf{y}_{n+1}=\mathbf{g}(\mathbf{x}_n,\mathbf{y}_n,c). \tag{1}$$

The drive $\mathbf{x}\in X$ and the response $\mathbf{y}\in Y$ are state vectors, X and Y are compact finite dimensional spaces, and both $\mathbf{f}$ and $\mathbf{g}$ are smooth or piecewise smooth maps. The parameter c characterizes the coupling or interaction strength. We expect that many of our observations hold in the case of bidirectionally coupled systems.[9,10] Unidirectionally coupled flows may be reduced to this form via a Poincaré or time-T map.

Generalized synchrony[2,7] is a useful concept in the analysis of coupled nonlinear systems, and is usually defined by the existence of a smooth, continuous map between the phase spaces X and Y of the two component systems. For our purposes, we will be concerned with the map $\phi:X\to Y$ which associates a *state* of the first system with a *state* of the second such that graph(ϕ) is invariant and attracting under the evolution of the coupled system.[11] Throughout this work, we will refer to the *synchronization set*, by which we mean graph(ϕ).[12] If the underlying dynamical equations have inherent symmetry, graph(ϕ) typically has a simple structure. For example, in the frequently studied case of coupled *identical* oscillators, the $\mathbf{x}=\mathbf{y}$ symmetry plane is invariant. In this

case, when the components are synchronized, trajectories are attracted to the plane of symmetry, and the synchronization set is trivial.

The continuity and smoothness of ϕ are important considerations, especially with regard to the practical detection of nonlinear synchronous states in experimentally obtained data. The existence of such states has been demonstrated in both physical[13] and biological systems.[6] However, we illustrate below that many systems of current interest exhibit synchronization sets with geometric complications that can have a detrimental effect on the detection of nonlinear synchrony from measured data. In particular, noninvertible coupled systems and systems lacking intrinsic symmetries can exhibit synchronization sets with very complicated structures. Since mismatches among coupled components are unavoidable—indeed heterogeneous coupled systems are of more general interest, especially when considering biological systems—a good understanding of the geometry of the synchronization sets of these more general systems is needed.

A closely related concept is *asymptotic stability*.[14] A unidirectionally coupled system is asymptotically stable if two (or more) identical copies of the response synchronize when subjected to the same driving signal. More precisely, for any two initial conditions $(\mathbf{x}_0,\mathbf{y}_0'),(\mathbf{x}_0,\mathbf{y}_0'')\in X\times Y$ which share the same initial drive state $\mathbf{x}_0$, we have $\lim_{n\to\infty}\|\mathbf{y}_n(\mathbf{x}_0,\mathbf{y}_0';c)-\mathbf{y}_n(\mathbf{x}_0,\mathbf{y}_0'';c)\|=0$, where $\mathbf{y}_n(\mathbf{x}_0,\mathbf{y}_0;c)$ is the y coordinate of the nth iterate of $(\mathbf{x}_0,\mathbf{y}_0)$ under the dynamics of the full system, and c is the coupling between the driver and response systems. This is similar to the idea of ''reliable response'' in the generation of neuronal signals.[15] Asymptotic stability and generalized synchrony are equivalent if the driving system is *invertible* and has a compact attractor.[16] We have observed, however, that it is possible to have asymptotic stability in systems which are noninvertible, for which graph(ϕ) is not even single-valued.[17]

In this paper we propose a categorization of the structures which arise in such synchronization states, and link these structures to specific features of the underlying dynamics. In Sec. II we describe and illustrate these categories using a general driver/response dynamical system. In Sec. III, two methods of quantifying these structures is presented, and we review the implications of these structures for the practical detection of synchronization from measured data. Concluding remarks appear in Sec. IV.

II. CATEGORIZATION

It is convenient to use a specific form of Eq. (1) to illustrate the various cases of interest. In the following, we take the driving system to be a modified baker's map and use a simple filter of one of the driver variables for the response. Specifically,

$$
\begin{aligned}
u_{n+1}&=\begin{cases}\lambda\,\omega(u_n,s), & v_n<\alpha,\\ \lambda+(1-\lambda)u_n, & v_n\geqslant\alpha,\end{cases}\\
v_{n+1}&=\begin{cases}v_n/\alpha, & v_n<\alpha,\\ (v_n-\alpha)/(1-\alpha), & v_n\geqslant\alpha,\end{cases}\\
y_{n+1}&=cy_n+\cos(2\pi u_{n+1}),
\end{aligned}
\tag{2}
$$

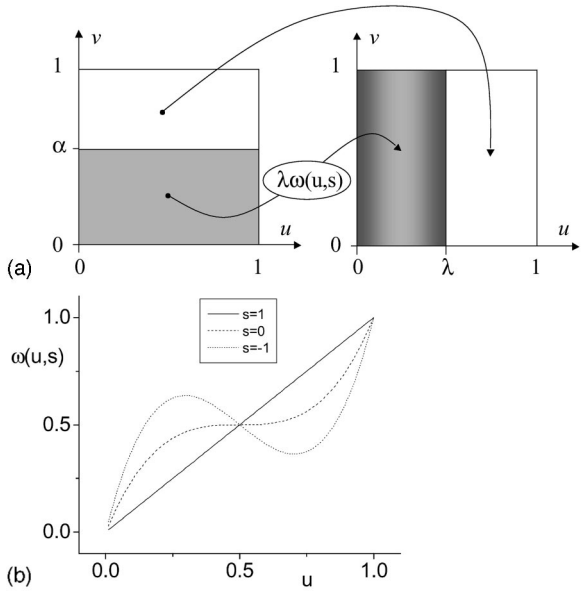

FIG. 1. (a) The modified generalized baker's map used as the driver in Eq. (2). The function $\omega(u,s)$ determines how the area of the lower rectangle in (a) is stretched and contracted horizontally, as schematically depicted by the shading. (b) Plot showing ω for three values of the parameter s.

where $0<\lambda<1$ and $0<\alpha<1$. The driver, by which we mean the (u,v) subsystem, maps the unit square into itself as illustrated in Fig. 1(a). The function $\omega(u,s)$ is a cubic polynomial in u defined by the following conditions: $\omega(0,s)=0$; $\omega(1,s)=1$; $\omega(1/2,s)=1/2$, and $\partial\omega/\partial u(1/2,s)=s$, where $-1\leqslant s\leqslant 1$. This function, graphed in Fig. 1(b) for various values of the parameter s, determines how the area within the lower rectangle of Fig. 1(a) is redistributed horizontally on each iterate. The response y is a filter of the drive's variable u with c controlling the transverse contraction rate. The parameter c, although technically not a coupling parameter in Eq. (2), is meant to model the more general case in which the dominant dynamical effect of coupling is to alter the contraction rate transverse to the synchronization set. One should also note that the limit at $c=0$ is sometimes singular. In particular, nontrivial synchronous structures such as cusps and multivalued sets described in the next section will persist for all values of c except at $c=0$. At $c=0$, the synchronization set collapses to the curve $y=\cos(2\pi u)$. Below, we vary s and c to obtain various synchronization sets with nontrivial geometric structures. In particular, we will be concerned with the map $y=\phi(x)$ which associates a *state* of the drive system with a *state* of the response such that graph(ϕ) is invariant and attracting under the evolution of the coupled system.

A. Wrinkling

The first type of nontrivial structure is best illustrated with $s=1$, so that $\omega(u,s)=1$ and the drive reduces to the standard baker's map. Referring to Fig. 1(a), this corresponds to uniform horizontal contraction and vertical stretching of the shaded rectangle. This case has been studied in Refs. 18 and 19, and we include it here for completeness.

If, in Eq. (2), $|c|<1$, the response is asymptotically stable for all $\mathbf{x}$. As pointed out in Refs. 18 and 19, the syn-

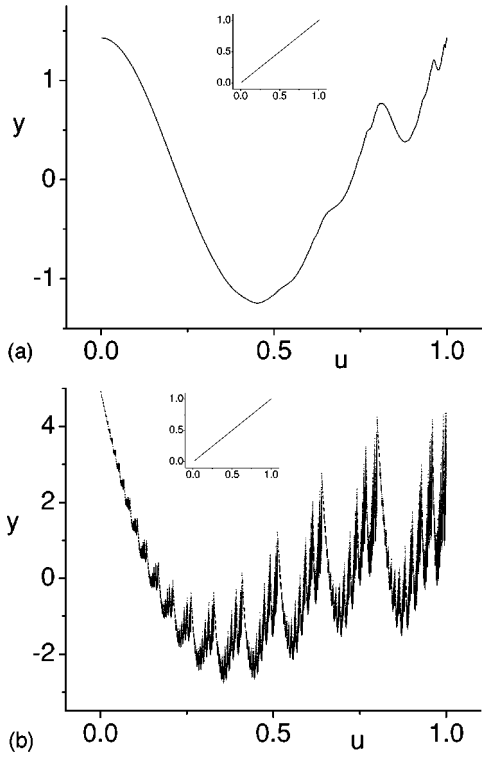

FIG. 2. Plots of the synchronization set of Eq. (2). The insets show the function ω. We set $s=1$, $\lambda=0.8$, and $\alpha=0.7$, for which $h_d=-0.64$. Note that $h_r=\ln c$. (a) Smooth case; $c=0.3$ and $|h_d|<|h_r|$; (b) wrinkled case; $c=0.8$ and $|h_d|>|h_r|$. The curve in (b) is Hölder continuous with exponent $|h_r/h_d|\sim 0.35$.

chronization set is typically not differentiable if the average contraction within the synchronization set (as determined by the drive) is larger than the contraction transverse to it (as determined by the response via c). In particular, let h_d be the most negative past-history Lyapunov exponent[20] of the drive and let h_r be the Lyapunov exponent corresponding to the transverse contracting direction. If $|h_r|<|h_d|$, then ϕ is generally not differentiable, but is only Hölder continuous with Hölder exponent[21] equal to $|h_r/h_d|<1$ at typical points.

Since the attractor of the generalized baker's map is uniform in v, the synchronization set can be accurately visualized in the uy plane. Graphs demonstrating both the differentiable and nondifferentiable cases are given in Figs. 2(a) and 2(b), respectively. We call the development of nondifferentiability in this fashion "wrinkling."

One can gain intuition about the wrinkling process by considering the following iterative geometric construction of the synchronization set. This construction is the essence of the graph transform method used first by Hadamard and later by a number of mathematicians to prove the existence of invariant manifolds.[22,23] Begin with the graph of $\cos(2\pi u)$ in the unit interval. (The choice of the initial curve is not important; any smooth curve with appropriate boundary conditions may be used.) Next, join two copies of the initial curve at $u=\lambda$, each scaled vertically by c and horizontally by λ and $1-\lambda$, respectively. Note that since the initial curve is periodic in the interval and its first derivative is zero at both ends, the combined curve is continuous in its value and its first derivative at the connection point. Finally, add graph($\cos(2\pi u)$) to the result to obtain the image of the initial curve under one complete iteration. Figure 3 illustrates the procedure. This entire process is then repeated to obtain further iterates of graph($\cos(2\pi u)$).

The above process produces a sequence of curves that limits to the synchronization set observed in Fig. 2. There are two competing factors responsible for the wrinkling. One is the vertical scaling factor c, which for $|c|<1$ tends to reduce the slope of the nth-stage curve. The other is the horizontal compression, which tends to increase this slope. Whether or not the slope at a given point in the limiting set is bounded depends on the competition between these two opposing factors. If the horizontal compression is stronger than the verti-

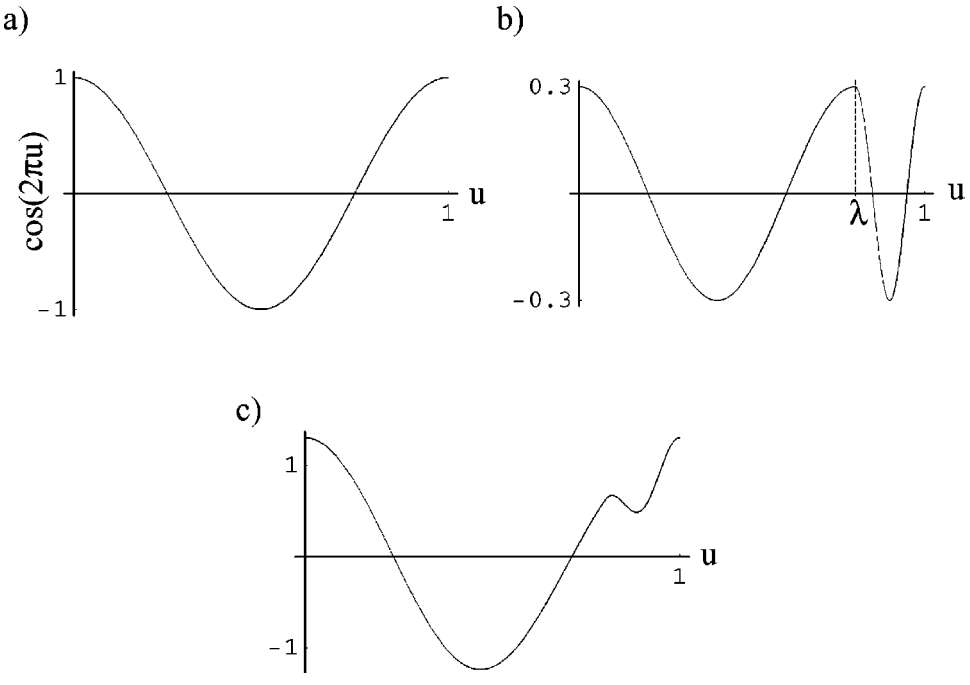

FIG. 3. Iterative geometric construction of the synchronization set of Eq. (2). (a) Begin with graph($\cos(2\pi u)$). (b) Two copies of the curve, each scaled vertically by c and horizontally by λ and $1-\lambda$ respectively, are joined at $u=\lambda$. $c=0.3$ and $\lambda=0.8$ are used for this example. (c) The resulting curve is then added to graph($\cos(2\pi u)$), giving the result shown (note the vertical scale). The process is then repeated.

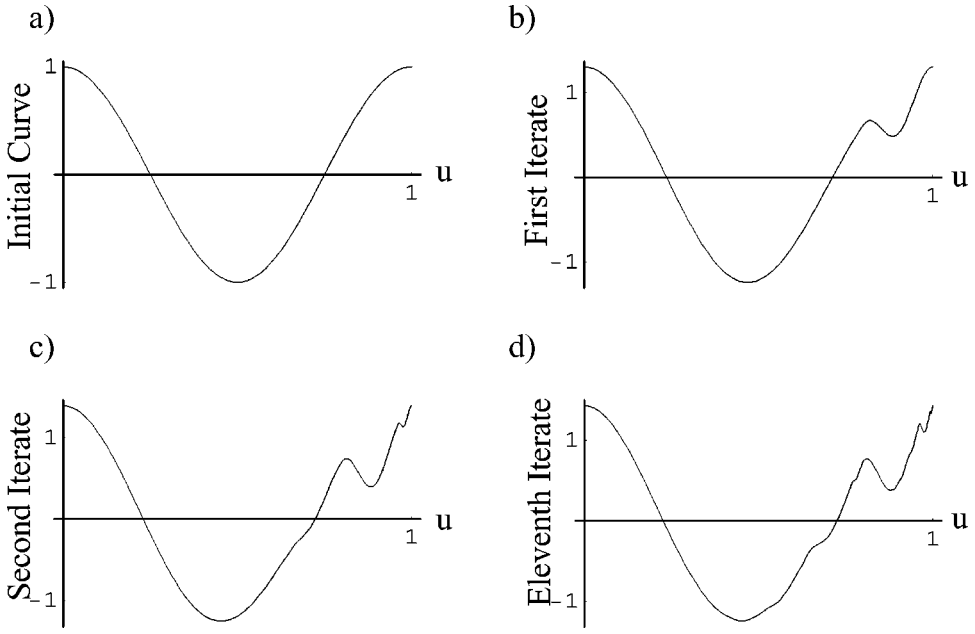

FIG. 4. Sequence of curves resulting from the iterative graph transform procedure for $\lambda = 0.8$ and $c = 0.3$ (smooth case). (a) Initial curve; (b) result after one iteration; (c) two iterations; (d) eleven iterations.

cal compression, the slope will tend to grow, and the curve in the limiting set will not be differentiable. Figures 4 and 5 illustrate the smooth and the wrinkled cases as sequences of curves generated by the graph transform procedure. In both sequences, the initial curve and the resultant curves after the first, second, and eleventh iterations are shown. (Movies showing the development of the synchronization set using the graph transform procedure are available on the web.[24]) As one can see from these two sequences, the iterated curves approach the actual synchronization set after only a few iterations. Note that the curve that is obtained after any finite number of iterations is differentiable (C^1), but the limiting curve in the wrinkled case is only Hölder continuous.

The wrinkling of the synchronization manifold is a *local* feature, and the smoothness in the vicinity of a single orbit depends on the ratio of the exponents h_r and h_d along this orbit. Thus there typically exist invariant sets embedded in the synchronization set on which ϕ has differing degrees of regularity. As we will demonstrate below, there are situations in which nondifferentiability on these smaller sets may become important. A quantification of this multifractality is given in Sec. III.

The degree of wrinkling is also closely connected to the concept of ''reliable response'' in the generation of neuronal signals. A system is said to respond reliably to an input if its response is identical each time the input is presented. (Experimental evidence for such behavior in neuronal tissue has been reported in Ref. 15.) Consider two trajectories beginning at nearby initial conditions in the drive system. The orbits of the drive will remain close to each other for a time $t \approx 1/h$, where h is the largest Lyapunov exponent of the driver. If the synchronization manifold is approximately

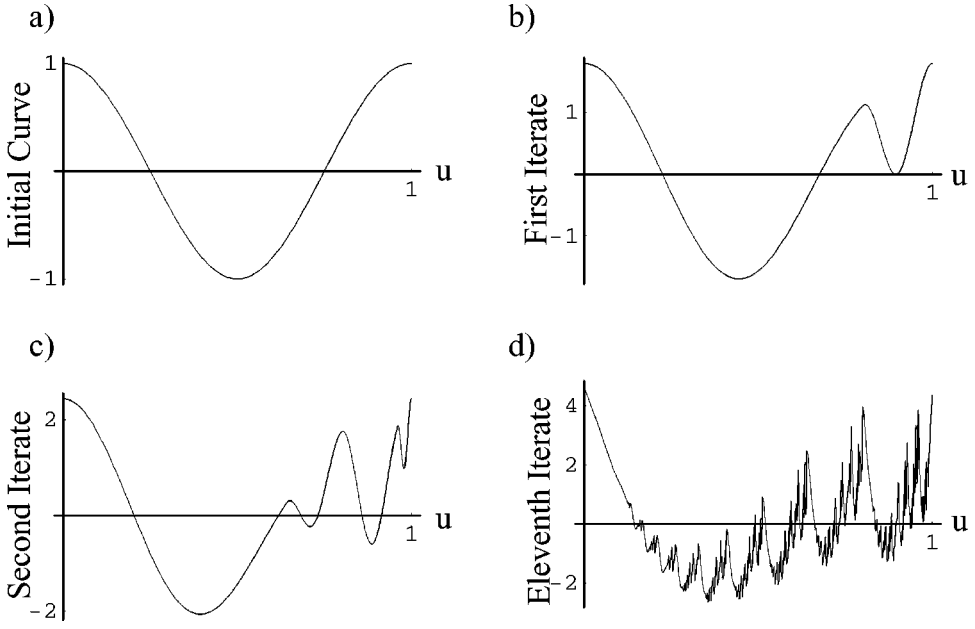

FIG. 5. Sequence of curves resulting from the iterative graph transform procedure for $\lambda = 0.8$ and $c = 0.8$ (wrinkled case). (a) Initial curve; (b) result after one iteration; (c) two iterations; (d) eleven iterations.

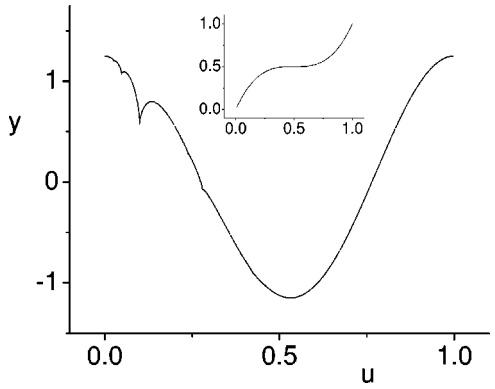

FIG. 6. Cusped case with $s=0$ and $c=0.2$. The inset shows the shape of ω. We set $\lambda=0.2$ and $\alpha=0.3$, for which $h_d=-0.90$ and $|h_d|<|h_r|$. Cusps occur at the forward iterates of the critical point at $u=1/2$ and decrease in size due to the cumulative effect of the transverse contraction.

smooth, then the difference between the two orbits of the drive will not affect the response system in significantly different ways during this time. However, if the synchronization set is severely wrinkled, then any small difference between the two states of the drive will be amplified in the response, even for times shorter than $1/h$. Thus, a reliable response cannot be expected.

B. Cusps

The second type of structure that can develop within the synchronization set results from the presence of critical points in the drive. At such a point the Jacobian matrix is singular, and we expect to find orbits in X near the critical points along which the contraction is arbitrarily large.

We illustrate this situation using the map in Eq. (2) with $s=0$. In this case, the contraction rate in the u direction is not uniform. Instead, ω, which remains invertible, has a critical (inflection) point at $u=1/2$, and thus the contraction rate along the line $u=1/2$ is infinite. As in the previous example, the synchronization set can be visualized as a graph in the uy plane. The result for the current case is shown in Fig. 6. We choose c sufficiently close to zero such that numerically, we find $|h_r/h_d|>1$ for a typical orbit. This suggests that graph(ϕ) is smooth almost everywhere. However, graph(ϕ) is not completely smooth, since ''cusps'' are formed at points corresponding to the orbits of $u=1/2$ that are affected by ω, i.e., that visit the shaded rectangles of Fig. 1(a). Thus, the main cusp occurs at $u=\lambda/2$. The next largest cusp occurs at $u=\lambda\omega(\lambda/2,0)$. More cusps appear at subsequent iterates, but these get progressively smaller in the figure because of the cumulative effect of the transverse contraction. Note that the Hölder exponent at each cusp is zero *regardless* of c. The significance of critical sets in general noninvertible maps in one and higher dimensions has been considered by Mira and co-workers (see Ref. 25, and references therein).

In addition, we have found through numerical means several periodic orbits sufficiently near cusps such that $|h_r/h_d|$ calculated along the orbit is less than one. We also expect that there are aperiodic orbits with the same property. For these orbits, however, the ratio $|h_r/h_d|$ depends on the value of c, and the size of the set of such points decreases as the rate of transverse contraction increases.

The iterative geometric construction discussed in the previous section applies to the current case with only one change: the horizontal rescaling is no longer linear, but is instead specified by $\lambda\omega$ for the left ''copy'' of the previous state. A sequence of pictures showing the first few stages in the construction of the synchronization set using the graph transform method is shown in Fig. 7. Beginning again with graph($\cos(2\pi u)$) as the initial condition, the resulting curve is seen to begin to resemble the actual synchronization set after only two iterations (compare Fig. 6).

Although graph(ϕ) is not smooth in either the cusped or the wrinkled case, its global structure in the two cases is different. The occurrence of wrinkling depends on the strength of the contraction rate in the direction transverse to

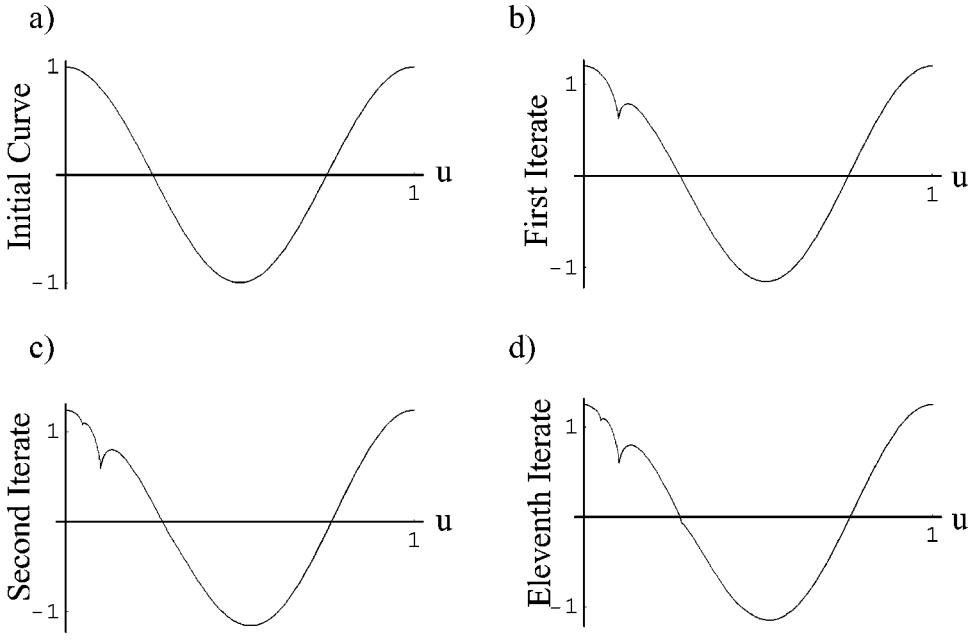

FIG. 7. Iterative geometric construction of the cusped synchronization set shown in Fig. 6. (a) The initial curve is graph($\cos(2\pi u)$); (b) result after one iteration; (c) two iterations; (d) eleven iterations.

the synchronization set. In particular, graph(ϕ) is everywhere differentiable for $c<\min(\lambda,1-\lambda)$ and is nonsmooth otherwise. In our second example, the function ω has a critical point at $u=1/2$ regardless of the value of c. Hence the driving system has a critical line, and the infinite contraction in the vicinity of this line (and its forward iterates) leads to cusps in the synchronization set where the Hölder exponent vanishes. We emphasize that this occurs for *all* values of c, in contrast to the first example. In addition, we expect in the cusped case that there is typically an additional small set of points along which the synchronization set is only Hölder, and that the size of this set decreases with increasing transverse contraction.

In Sec. III, we introduce statistics which describe the differences between these two cases in a more quantitative fashion.

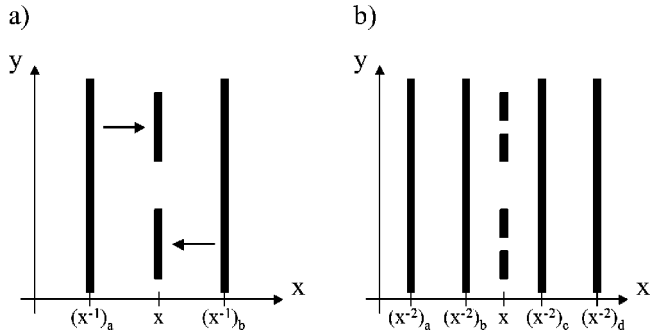

FIG. 8. The connection between multivalued synchronization sets and noninvertibility. (a) The state **x** of the drive has two preimages under f as shown. Each preimage is then associated with all possible response values **y**; this situation is then iterated forward under the full dynamics **F**. The result is two typically disjoint sets of **y** values, both associated with the drive state **x**. (b) The same argument considering two steps into the past.

C. Multivalued synchronization sets

In this section we discuss the development of multivalued synchronization sets. Such structures are associated with the presence of noninvertibility in the underlying equations. Noninvertible mathematical models are very important in nonlinear dynamics, despite the usual assumption that physical processes are fundamentally described by inherently invertible ordinary differential equations. The use of the logistic map in the study of population dynamics in biology[26] is a well-known example. More generally, dynamics reconstructed from measured time series of systems with strong dissipation are frequently best and most usefully approximated by noninvertible maps.[27] Models with time-delays, important for describing neuronal and more general biological processes, are even more complicated since a proper description requires delay differential equations; temporal invertibility in these systems cannot be taken for granted.[28]

The synchronization set can be characterized as the set of points that have preimages within the box $X\times Y$ N steps into the past for every positive integer N. That is, a point **(x,y)** is in the synchronization set if $\mathbf{F}^{-N}$**(x,y)** stays within the box $X\times Y$ for every positive integer N.[29,30] From this point of view, the connection between the multivalued nature of a synchronization set and noninvertibility can be understood as follows. A noninvertible drive implies that there are drive states that have more than one inverse image under **f**. Consider such a drive state **x**. Associate the set of all possible **y** values with each of the preimages of **x**. Typically, these iterate forward under **F** to a disjoint union of sets of **y**-values associated with **x** such that each component of this union corresponds to one preimage of **x**. This is depicted schematically in Fig. 8(a). The above argument may be repeated using the set of preimages under **f** of drive state **x** j steps into the past, for $j=2,3,\ldots$. This yields a disjoint union of an increasing number of smaller sets of **y**-values that is associated with the drive state **x**, as shown in Fig. 8(b) for $j=2$. Thus, ϕ is multivalued. Intuitively, each particular jth preimage of **x** gives rise to a different orbit that lands on **x** after j iterates. These different trajectories (also called histories) provide different driving signals to the response system, and therefore, once the drive lands on **x**, the response can be in any of several possible states. Multivalued synchronization sets have been described in Refs. 8 and 17 and observed experimentally in Ref. 31. A different and less severe form of multivalued synchronization, in which the drive and response are related by a $1:m$ ratio, has been recently reported.[32,33]

We now give several examples of this phenomenon. First, we note that the driver in Eq. (2) is noninvertible when ω has a negative slope at $u=1/2$, i.e., for $s<0$. The synchronization set for $s=-1/2$ is illustrated in Fig. 9. Note that as s is progressively decreased from 1 to 0 to $-1/2$, the synchronization set goes from being smooth to having cusps; the cusps then ''push through'' to form loops. Thus the synchronization set becomes multivalued. An animation of this process is available on the web.[24]

The development of the multivalued synchronization set in this case is particularly clear in terms of the iterative geometric construction described above. Beginning again with the graph of $\cos(2\pi u)$, the first step in the construction is to rescale this curve vertically by c and horizontally by $\lambda\omega$. The latter step can be thought of as occurring in three separate pieces as indicated in Figs. 10(a) and 10(b); the result is the formation of the looped curve shown in Fig. 10(c). This is then joined to another copy of the original curve which is

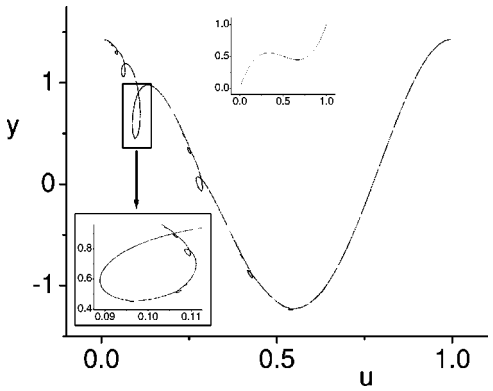

FIG. 9. Multivalued ''looped'' case with $s=-0.5$ and $c=0.3$. The upper inset shows the shape of ω. We set $\lambda=0.2$ and $\alpha=0.3$, for which $h_d=-0.7$ and $|h_d|<|h_r|$. The lower inset magnifies the largest loop, in which additional loops, going both inward and outward, are evident. The apparent gaps in the curve are due to finite iteration.

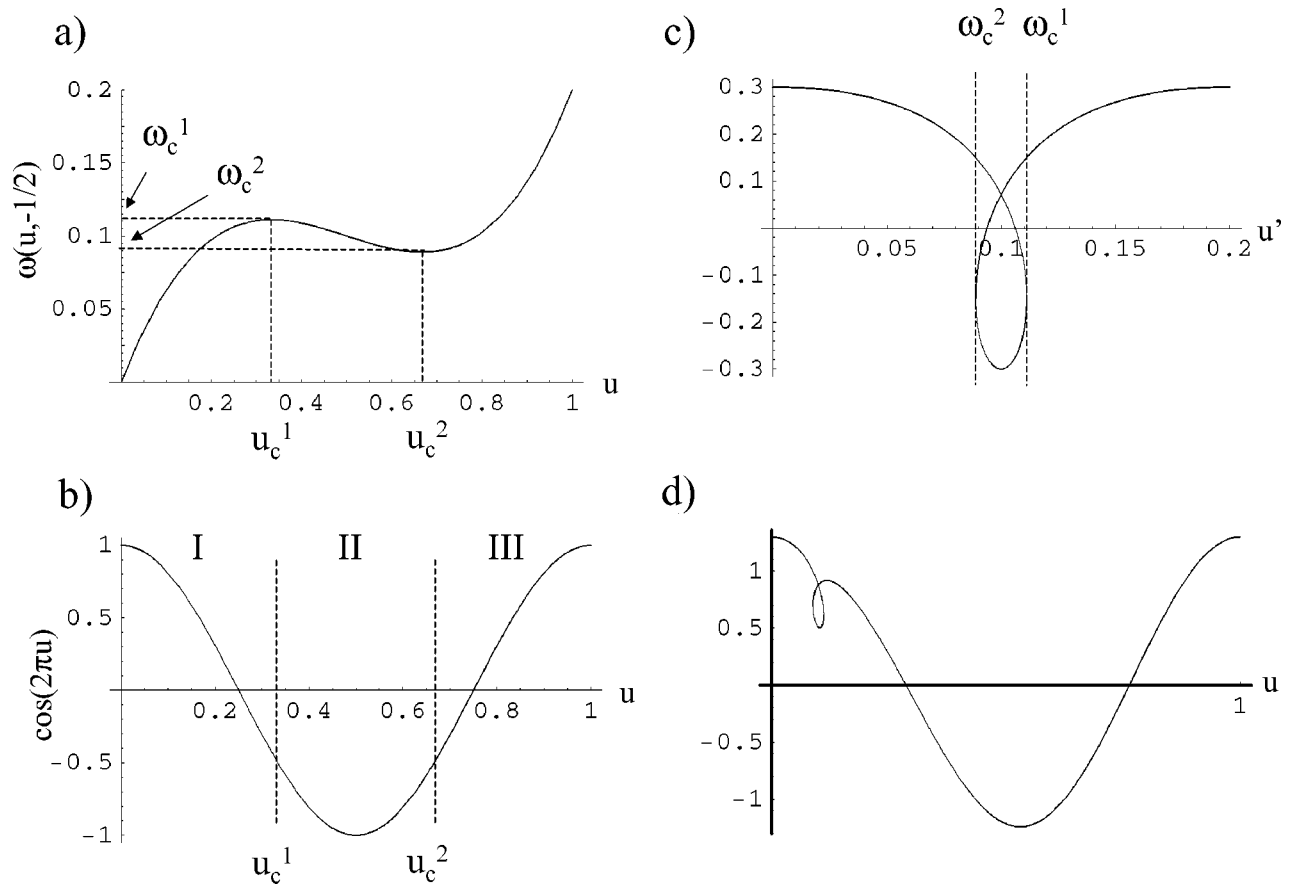

FIG. 10. Iterative geometric construction of the multivalued synchronization set shown in Fig. 9. (a) The function $\omega(u,-1/2)$, which is noninvertible, has two critical points at u_c^1 and u_c^2 as shown. The images of these critical points under the cubic function $u'=\omega(u,-1/2)$ are ω_c^1 and ω_c^2. (b) The initial curve $\cos(2\pi u)$ in the iterative process. It is useful to consider the horizontal stretching and contraction by the factor $\lambda\omega$ as occurring in three pieces as shown. Specifically, the curve in region I maps to the curve starting from $u'=0$ to $u'=\omega_c^1$; the curve in region II maps to the U shaped curve in reverse order within the domain $u'\in[\omega_c^2,\omega_c^1]$; and the curve in region III maps to the curve starting from $u'=\omega_c^2$ to $u'=1$. The result is shown in (c). To complete one cycle of the iterative process, the curve resulting from part (c) is added to graph($\cos(2\pi u)$), giving the result shown in (d). The process is then repeated.

scaled uniformly both vertically and horizontally, and the result is added to graph($\cos(2\pi u)$). The curve after one full step of the iterative process is shown in Fig. 10(d). Note that in the course of iteration, it is possible to obtain loops within loops. This feature is evident in Fig. 9; see the lower inset, which enlarges the main loop.

Another way to introduce noninvertibility into Eq. (2) is to allow the rectangles depicted in Fig. 11 to overlap. Recall that for $s=1$, the driver in Eq. (2) reduces to the standard baker's map. Rewriting this system to explicitly account for the overlap, we consider the following system:

$$u_{n+1}=\begin{cases}(\lambda+\rho(1-\lambda))u_n, & v_n<\alpha,\\ (1-\rho)\lambda+(1-(1-\rho)\lambda)u_n, & v_n\geqslant\alpha,\end{cases}$$
$$v_{n+1}=\begin{cases}\dfrac{v_n}{\alpha}, & v_n<\alpha,\\ \dfrac{v_n-\alpha}{1-\alpha}, & v_n\geqslant\alpha,\end{cases} \tag{3}$$
$$y_{n+1}=cy_n+\cos(2\pi u_{n+1}),$$

where $\rho\in[0,1]$ determines the degree of overlap. Figures 11(a) and 11(b) show the synchronization sets that result for $\rho=0.3$ and $\rho=0.8$ with $c=0.3$.

We now give an example for which the synchronization set is multivalued for all drive states, and the structure can be understood exactly. Consider the following two-dimensional piecewise linear system:

$$x_{n+1}=f(x_n)=\begin{cases}2x_n, & x_n<0.5,\\ 2(x_n-0.5), & x_n\geqslant 0.5,\end{cases}$$
$$y_{n+1}=g(x_n,y_n,c)=cy_n+x_{n+1}, \tag{4}$$

where f is noninvertible with two preimages for each x_{n+1}. For $|c|<1$, the system is asymptotically stable. Figure 12 shows the synchronization set, which consists of a set of lines. The topology in this case is unusual because the drive is not continuous; we expect that for the more typical case of a continuous noninvertible drive-response system, the synchronization set will be connected. However, we believe that the one-to-many structure illustrated by this example is typical of many cases.

The structure of this synchronization set can be understood using a linear transformation of the full (x,y) system. In particular, let $(\tilde{x}\ \tilde{y})^{\mathrm{T}}=\mathbf{T}(x\ y)^{\mathrm{T}}$, where

$$\mathbf{T}(c)=\begin{pmatrix}1 & 0\\ -2(1-c)/c & (2-c)(1-c)/c\end{pmatrix}. \tag{5}$$

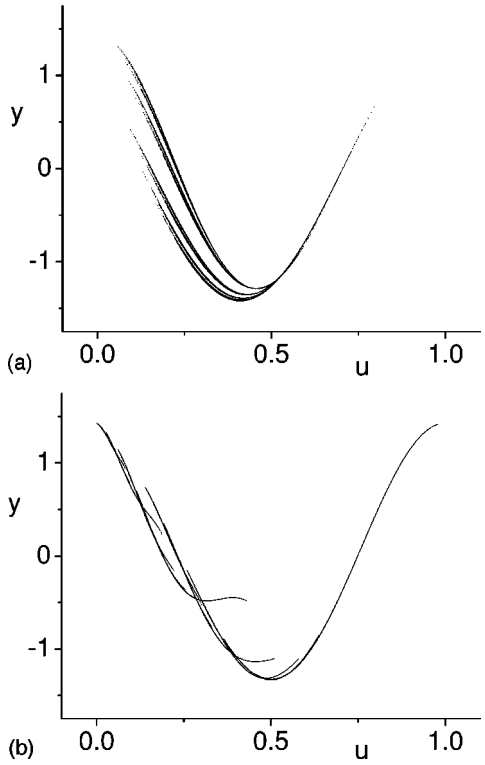

FIG. 11. The multivalued synchronization sets resulting from Eq. (3) for (a) $\rho=0.3$ and (b) $\rho=0.8$. In both cases, $c=0.3$.

In the new coordinates, Eq. (4) becomes the ''skinny'' baker's map given by

$$\tilde{x}_{n+1}=\begin{cases}2\tilde{x}_n, & \tilde{x}_n<0.5,\\ 2(\tilde{x}_n-0.5), & \tilde{x}_n\geqslant 0.5,\end{cases}$$

$$\tilde{y}_{n+1}=\begin{cases}c\tilde{y}_n, & \tilde{x}_n<0.5,\\ c\tilde{y}_n+(1-c), & \tilde{x}_n\geqslant 0.5.\end{cases} \tag{6}$$

Under one iteration, the two halves of the unit square are mapped into two horizontal rectangles as shown in Fig. 13. For $c<1/2$, this map contracts area at a rate given by $2c$. After n iterations, the original unit square is mapped into 2^n horizontal strips of height c^n, and the limiting set of this process is a Cantor set of lines. The attracting set of the original map (Fig. 12) is the image of this Cantor set of lines under the transformation $\mathbf{T}^{-1}(c)$.

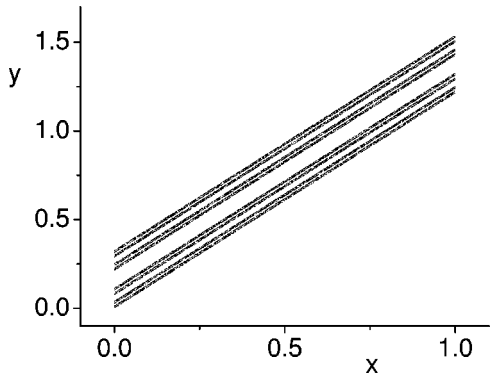

FIG. 12. The synchronization set of Eq. (4) with $c=0.35$.

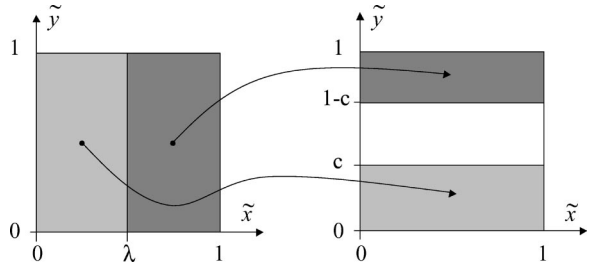

FIG. 13. The skinny baker's map.

This example also demonstrates how a multivalued synchronization structure is directly related to the history of the drive. In terms of the thin baker's map, one particular history of a drive state $\tilde{x}_n$ can be uniquely described by a sequence of the symbols R and L, constructed by listing an L each time that a preimage lands to the left of $\tilde{x}=1/2$, and an R each time that a preimage lands to the right of $\tilde{x}=1/2$. An illustration is given in Fig. 14 in which we have drawn the images of two halves of the unit square as we iterate Eq. (6) forward twice. At the end of the second iteration, we can associate different symbol sequences with the points $(\tilde{x}_n(i),\tilde{y}(i))$ $(i=1,\ldots,4)$, where each such point is located within a different horizontal strip and all correspond to the same $\tilde{x}$ value at time n. A finer resolution of the striated strips corresponds to additional steps backwards in time, which in turn corresponds to more symbols in the symbol sequence. Each point has a distinct infinite symbol sequence. Using a metric on the space of symbol sequences, one can also determine the difference between the orbits of any two striations. Two striations are close together if the most recent symbols in the sequence are identical.

The case of a noninvertible drive discussed in this section may be reduced to the case with an invertible driver at the expense of replacing the driving system with one that is more complex. Let $\Omega=(X,\mathbf{f})$ be the space of all infinite sequences $(x_0,x_1,\ldots)$ such that $x_i=\mathbf{f}(x_{i+1})$ (the inverse limit

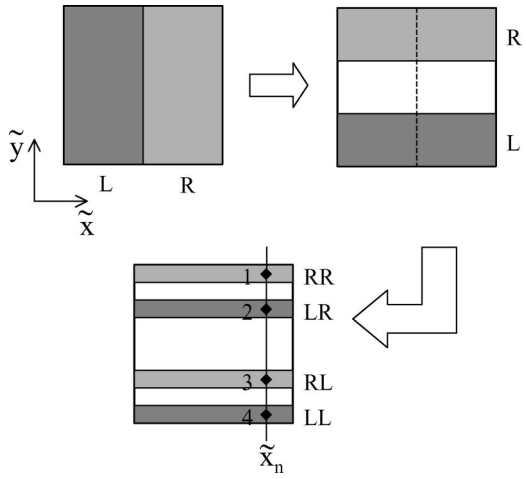

FIG. 14. Dynamics under the skinny baker's map of Eq. (6). Top left: The original domain is divided into regions R and L. Top right: The image of R and L after one iterate. Bottom: After two iterates, the original region R maps to the regions labeled RL and RR, and the original region L maps to the regions labeled LL and LR.

space). We define an *invertible* map $\hat{\mathbf{f}}$ on Ω by $\hat{\mathbf{f}}(x_0,x_1,\ldots)=(\mathbf{f}(x_0),x_0,x_1,\ldots)$. It is easy to check that the response system in Eq. (1) and the response system in

$$\hat{x}'=\hat{\mathbf{f}}(\hat{x}),$$
$$y'=g(\pi_0(\hat{x}),y), \tag{7}$$

receive the same input, where $\pi_0(\hat{x})=x_0$ is the projection of the sequence $\hat{x}$ onto its first coordinate. Therefore, the dynamics of these response systems is the same in both cases. The driving system in Eq. (7) is invertible, and thus the graph transform method converges to a single-valued map $\hat{\phi}:\Omega\to Y$. The multivalued function ϕ whose graph is the synchronization set in Eq. (1) can be obtained by projecting graph($\hat{\phi}$) onto the first coordinate.

The complexity of the synchronization set becomes apparent when the topology of this inverse limit space Ω is analyzed. This space has an extremely complicated structure even in the relatively simple case of unimodal maps of the interval.[34] To get a better description of the synchronization set, we briefly outline an extension of the idea of symbol sequences introduced in the case of the ''skinny'' baker's map. The construction of systems with invertible drivers on inverse limit spaces will be addressed in more detail elsewhere.

We will describe this method in the case of the tent map f of the interval $I=[0,1]$ with critical point 1/2, and such that $f(1/2)=1$. The critical point separates the interval into subintervals $I_1^1=[0,1/2]$ and $I_2^1=[1/2,1]$. The preimage of each of these intervals consists of the intervals I_1^2, I_2^2 and I_3^2, I_4^2 such that $f(I_1^2)=f(I_2^2)=I_1^1$ and $f(I_3^2)=f(I_4^2)=I_2^1$. This process can be continued to create a tree of intervals such that a pair of intervals on the $(n+1)$-st level of the tree maps to an interval in the nth level of the tree.

If the map f defines the driving map of the system in Eq. (1), the graph transform method can be performed on infinite paths starting at any node I_m^n in this tree of intervals. The method converges to a function $\phi_m^n:I_n^m\to Y$ over the first interval in such a path. The graphs of these functions are not invariant themselves, however, under the dynamics of Eq. (1), graph(ϕ_m^n) maps into graph($\phi_{m'}^{n-1}$) when $f(I_m^n)=I_{m'}^{n-1}$, and thus the family $\{\text{graph}(\phi_n^m)\}_{n,m}$ is an invariant family of graphs. Moreover the graphs in this family are joined over the points in the history of the critical point 1/2, i.e., over the points $k/2^n$.

This idea can be extended to describe the invariant sets over more complicated driving systems. In the case of Eq. (2), we again obtain a family of graphs which are joined over the orbits of the critical points. If the map of the driving system is smooth, we again encounter the problems discussed in Sec. II B, since the contraction becomes very large close to the orbits of the critical points. Thus, smoothness of the graphs in the invariant family cannot be expected at any orbit that is close to the orbit of the critical point over sufficiently many iterates.

We conclude this section by stressing that the multivalued structure of the synchronization set for all these cases is an intrinsic feature of the underlying dynamics resulting from the presence of noninvertibility. Thus, we expect that the multivalued nature of $\phi(x)$ persists for almost all values of c.

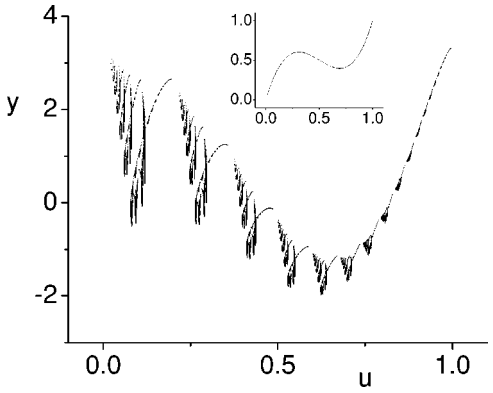

FIG. 15. A multivalued and wrinkled synchronization set obtained from Eq. (2) with $\lambda=0.2$, $\alpha=0.3$, $s=-0.8$, and $c=0.7$.

D. Combinations

Finally, we briefly note that the various cases described above can coexist. For example, Fig. 15 shows a case that is both multivalued and wrinkled; this is obtained using Eq. (2) and setting $\lambda=0.2$, $\alpha=0.3$, $s=-0.8$, and $c=0.7$. Furthermore, since a smooth noninvertible map must have critical points, the situations described in Sec. II B and Sec. II C should be expected to occur together.

Animations showing the evolution of the synchronization set as both s and c are varied are available on the web.[24]

III. QUANTIFICATION

Here we present two methods for quantifying the features of the synchronization set that we have described above.

A. $\epsilon_{\max}-\delta$ test

Most practical methods of detecting nonlinear synchrony in data rely strongly on the continuity of ϕ, and in general also require a certain degree of smoothness of ϕ.[5–7] These methods generally proceed by checking if clusters of points in X correspond to similarly small clusters of points in Y. It is important to note that the presence of the intrinsic geometric features that we have discussed above can significantly hinder the experimental detection of more complicated (and perhaps more interesting) synchronous relationships.

Consider the following numerical test based on the definition of continuity. Iterate the system of interest [e.g., Eq. (1)] for a sufficiently long time to allow transients to die out. Pick a point $(\mathbf{x},\mathbf{y})$ on the attractor and a small number δ, and iterate the full system until the $\mathbf{x}$-component of the trajectory lands in the ball $B_{\mathbf{x}}(\delta)$ a large number of times. Keep track of these points, and let $\epsilon_{\max}$ denote the largest distance between the corresponding $\mathbf{y}$-components. If ϕ is differentiable, then typically $\epsilon_{\max}\to 0$ linearly as $\delta\to 0$. When $|h_d|>|h_r|$, the function ϕ is typically only Hölder continuous, and $\epsilon_{\max}\to 0$ sublinearly as δ decreases. The Hölder exponent of ϕ at $\mathbf{x}$ can be estimated from the slope of the graph of

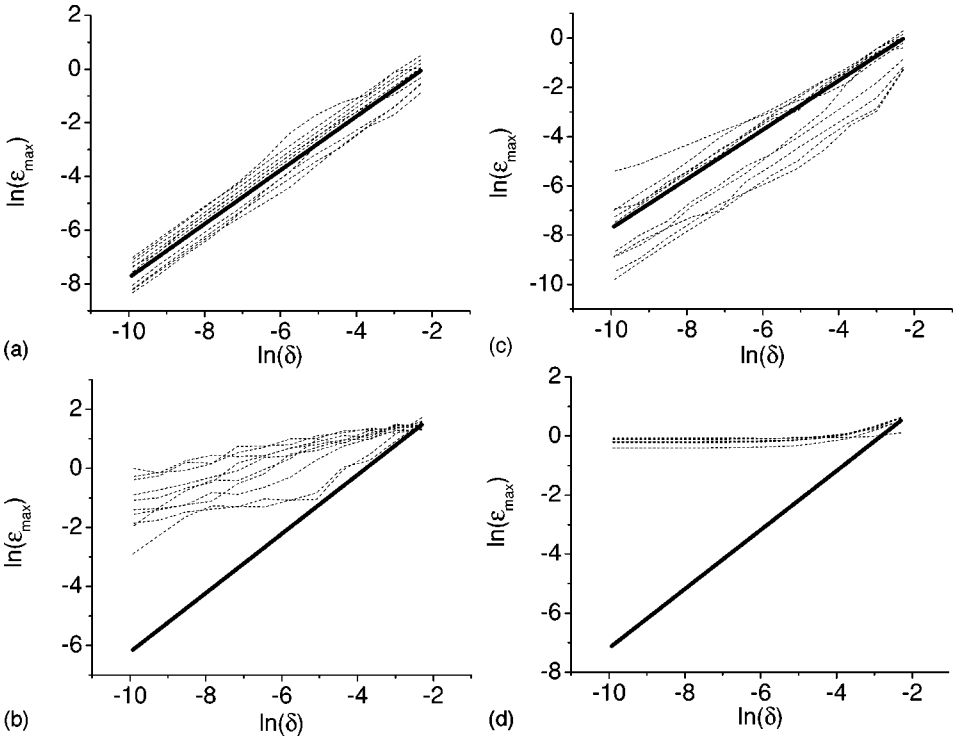

FIG. 16. Graphs of $\ln(\epsilon_{\max})$ versus $\ln(\delta)$ for Eq. (2). In each case, several curves are shown, corresponding to several randomly chosen fiducial points in the driver. The thick line has slope 1. The graphs correspond to (a) the smooth case in Fig. 2(a); (b) the wrinkled case in Fig. 2(b); (c) the cusped case in Fig. 6; and (d) the multivalued (looped) case in Fig. 9.

$\ln(\epsilon_{\max})$-$\ln\,\delta$, and to probe the overall smoothness of the synchronization set, an ensemble of scaling curves with randomly chosen fiducial points **x** can be studied.

Figures 16(a)–16(d) show the results of applying this process to the various cases considered above. First, consider the smooth/wrinkled transition discussed in Sec. II A, in which $s=1$ in Eq. (2). When $|h_d|<|h_r|$, ϕ is smooth almost everywhere, and the $\ln(\epsilon_{\max})$–$\ln\,\delta$ curves have slope 1, as shown in Fig. 16(a). In contrast, when $|h_d|>|h_r|$, the synchronization set is only Hölder continuous and thus ϕ is not differentiable almost everywhere. The scaling curves therefore have smaller slopes, as shown in Fig. 16(b). For this case, synchronization detection methods may not be able to detect synchronization at all, even in the absence of noise.

In the cusped case, cusps of decreasing size occur at (and near) forward iterates of $u=1/2$ for all c. However, the synchronization set may be otherwise smooth, depending on c. Thus, the $\ln(\epsilon_{\max})$–$\ln\,\delta$ graphs show a variety of slopes depending on the location of the fiducial point **x**; see Fig. 16(c). While most curves have slope 1, a few have smaller slopes. In this case, standard synchrony detection methods fail to detect the presence of the cusps.

Figure 16(d) demonstrates the effect of the multivalued structure of Eq. (4) (Fig. 12) on the $\ln(\epsilon_{\max})$–$\ln\,\delta$ graphs. These are seen to saturate at a scale that corresponds to the ''thickness'' of the synchronization set. As a consequence, the ability to predict the state of the response system from the state of the drive is severely affected, and this situation cannot be improved by increasing the precision of the measurements. Although there is a dynamically coherent relationship between the driver and the response (in fact, the system is asymptotically stable), most synchronization detection methods will fail to detect any synchronous relationship in such multivalued cases.

B. Wavelets

As shown in Sec. II A, the Hölder exponent of ϕ at a point **x** depends on the ratio of two contraction rates, and can therefore vary from point to point. This is characteristic of a multifractal set. In this section we use the wavelet methods described in Ref. 35 as a more accurate way to examine the regularity of multifractal synchronization sets. In particular, we are interested in estimating the typical Hölder exponents, i.e., those that occur on some set of full measure, as well as the distribution of other, nontypical exponents. The details of this method are briefly discussed in the Appendix, and the interested reader is referred to the literature on the estimation of the regularity of functions using wavelet techniques.[35,36] Since the function $\phi(u,v)$ obtained from Eq. (2) is constant in the v direction, we will keep v constant in our analysis and treat ϕ as a function from the real line to itself.

The wavelet transform may be thought of as a space-localized counterpart of the Fourier transform. The Fourier transform decomposes a function into sinusoidal components of varying frequency, which are not localized in space. In contrast, the wavelet transform decomposes a signal into a family of wavelets of varying location and size $\Psi((u-b)/a)$. All the wavelets in such a family are obtained from a single function $\Psi(u)$, which is shifted by b and dilated by a factor a. The ''mother wavelet'' $\Psi(u)$ is typically chosen to be localized in space, so that we can think of the wavelet transform as a microscope magnifying an area around $u=b$ by a factor a.

A smooth function looks nearly constant after sufficient magnification, and hence the coefficients of the wavelets needed to describe such a function at small scales are vanishingly small. On the other hand, cusps or wrinkles persist under magnification, and hence wavelets of all sizes are

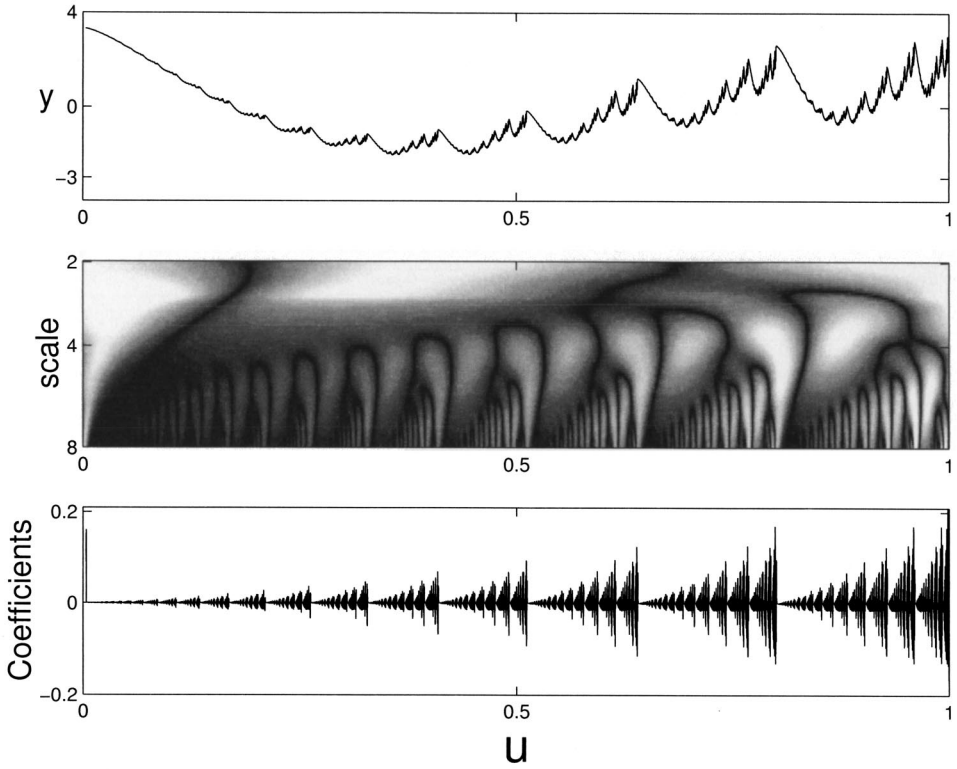

FIG. 17. The wavelet transform of the wrinkled ϕ discussed in Sec. II A. The middle figure represents the wavelet coefficients at different scales. The light regions correspond to large wavelet coefficients. Wavelet coefficients for $a=2^{12}$ are plotted in the bottom figure. Note that the self-similarity of the graph is reflected in the wavelet coefficients. We have used Matlab routines from the package WaveLab in the analysis presented in Figs. 17–20.

needed to describe a function around such points. It can be shown that, for appropriately chosen wavelets, the wavelet coefficients scale as

$$W_{\Psi}(u_0,a)\sim a^{h(u_0)}$$

at a point u_0, where a is the scaling factor of the wavelet and $h(u_0)$ is the Hölder exponent of the function at that point.[35,36] Unlike the Fourier transform, which can be used to give general information about the roughness of a function, this fact allows us to use wavelets to estimate the local roughness of a function.

These ideas are illustrated in Figs. 17 and 18. In Fig. 17 we have chosen the wrinkled synchronization set discussed in Sec. II A. The white regions show regions of high wavelet

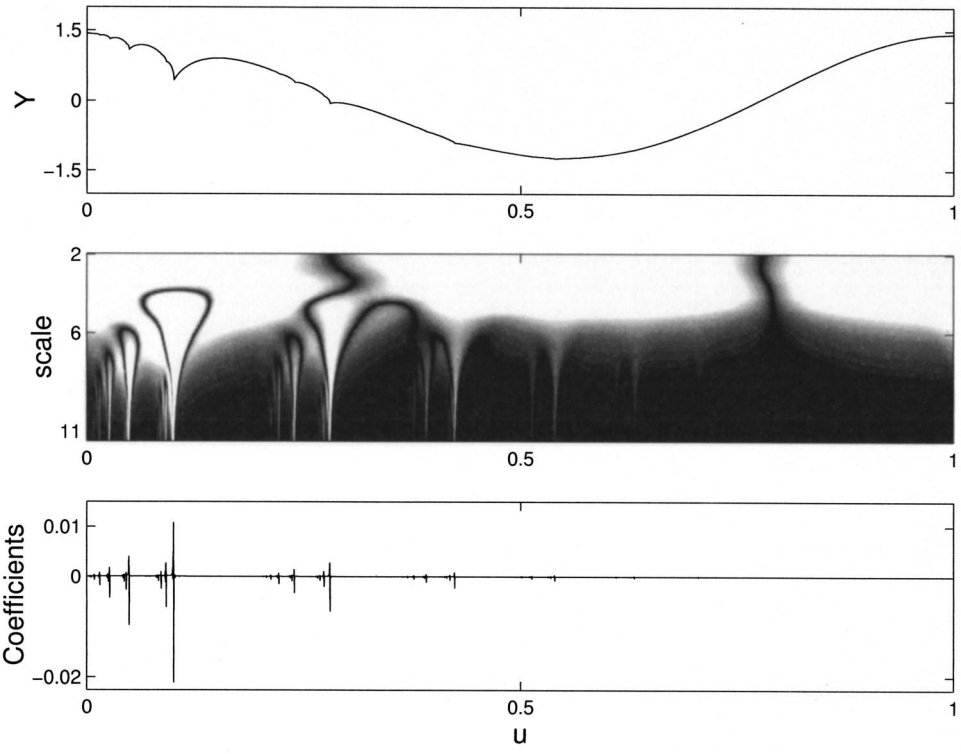

FIG. 18. The wavelet transform of the cusped ϕ discussed in Sec. II B. The graphs are the same as in Fig. 17.

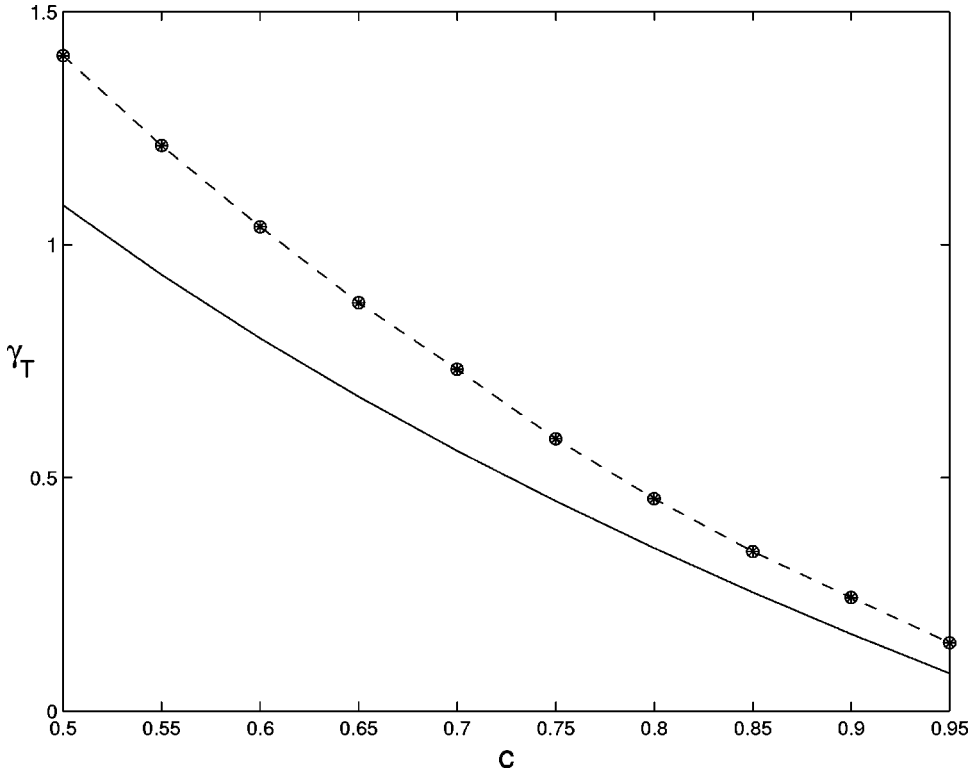

FIG. 19. The typical smoothness of the synchronization manifold as a function of the coupling strength c. The solid line is obtained from the theoretical prediction, while the dashed line is obtained from the wavelet transform. For any finite resolution level, the wavelet method provides an upper bound for γ_t which is consistent with the observed numerical overestimate.

coefficients. Note that the graph of the wavelet coefficients reveals the self-similar structure of the graph. The wavelet coefficients computed for the cusped case of Sec. II B are shown in Fig. 18. In this case, the cusps are distributed very sparsely, but occur at many different scales.

Returning to the wrinkled case of Sec. II A, in which setting $s=1$ in Eq. (2) reduces the drive to the baker's map, the typical past-history Lyapunov exponent in the contracting direction is given by

$$h_d=\alpha\ln\lambda+(1-\alpha)\ln(1-\lambda)<0, \tag{8}$$

and the response Lyapunov exponent is $h_r=\ln c$.[18] Therefore, the typical Hölder exponent γ_t of the synchronization set is

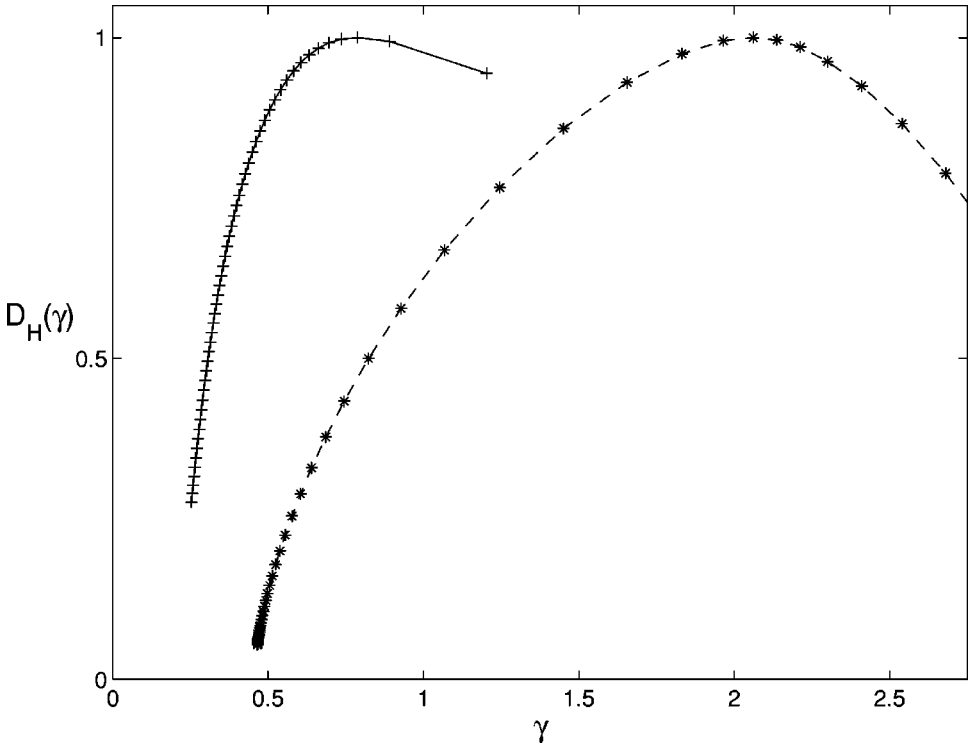

FIG. 20. The functions $D_H(\gamma)$ for the wrinkled case with $c=0.7$, $\alpha=0.7$, and $\lambda=0.8$ (solid line), and for the cusped case with $c=0.2$, $\alpha=0.3$, and $\lambda=0.2$ (dashed line). In the wrinkled case $\gamma_{\min}\approx 0.2$ is predicted correctly. In the cusped case due to the sparsity of cusps, it is difficult to compute $D_H(\gamma)$ numerically for small Hölder exponents.

$$\gamma_t = \frac{\ln c}{\alpha \ln \lambda + (1-\alpha)\ln(1-\lambda)}. \quad (9)$$

In Fig. 19, γ_t computed numerically as a function of c is compared with the results obtained analytically from Eq. (9).

The smallest (largest) Hölder exponent on the synchronization set corresponds to points whose orbits lie entirely in the part of the square which is more contracting (less contracting). Therefore, we obtain $\gamma_{\min} = \ln c/\ln \lambda$ and $\gamma_{\max} = \ln c/\ln(1-\lambda)$ if $\lambda > 1/2$. The Hölder exponents of ϕ therefore range from $\gamma_{\min}$ to $\gamma_{\max}$, and are equal to γ_t on a set of full measure.

We introduce the dimension $D_H(\gamma)$ of the set of all points in the domain of ϕ at which ϕ is Hölder with exponent γ. Since $D_H(\gamma_{\min}) = D_H(\gamma_{\max}) = 0$ and $D_H(\gamma_t) = 1$, this function varies between 0 and 1. As explained in the Appendix, wavelets provide a natural way of computing $D_H(\gamma)$ as a function of γ. The function $D_H(\gamma)$, frequently called the singularity spectrum $f(\alpha)$, is expected to have a characteristic $\cap$ shape, hitting zero at $\gamma_{\min}$ and $\gamma_{\max}$ and attaining a maximum at γ_t. The γ_t in Fig. 19 were obtained by computing $D_H(\gamma)$ numerically for each c, and finding the maxima.

In Fig. 20 we show the $D_H(\gamma)$ functions for a wrinkled and a cusped synchronization set. Note that the peak of $D_H(\gamma)$ in the cusped case is to the right of 1, showing that the function is differentiable on a set of Hausdorff dimension 1. The function corresponding to the wrinkled case shows that the ϕ is only Hölder continuous on a set of Hausdorff dimension 1.

The wavelet analysis of signals presented here provides a computationally robust estimation procedure, and is more systematic than the method described in the previous section. Moreover, the graphical display of the singularity spectrum is an interpretable way of quantifying the irregularities of the signal. Using these methods it is possible to make statistical distinctions between different signals. This idea has been successfully used to distinguish between signals in biomedical applications.[37]

IV. CONCLUSION

In summary, we have shown that for coupled systems without symmetries, systems can be coherent without having easily-detectable synchronization properties. We have given examples of invertible and noninvertible drivers for which the system is asymptotically stable, yet the synchronization set is nonsmooth or multivalued. We have given an example of a test for synchrony which incorporates features of most standard tests. We illustrate the misleading nature of the outcome of this test (and most standard tests) when it is applied to synchronization sets containing the complicated features of our examples. Furthermore, we give a sophisticated method of detection designed for multifractal synchronization sets. These coherent yet complicated structures might affect the generation of ''reliable response'' in neuronal pathways within actual biological systems. In conclusion, we emphasize that complicated synchronization sets and their practical implications are not pathological: asymmetry and noninvertibility are typical in many biological and physical systems.

ACKNOWLEDGMENTS

The authors gratefully acknowledge helpful conversations with S. J. Schiff, and support from the following sources: NIH 1K25MH01963 (E.B.); a George Mason University College of Arts and Sciences Junior Faculty Award (E.S.); NSF-IBN 9727739 and NIH 2R01MH50006 (P.S.).

APPENDIX: WAVELET FORMALISM

In recent years much research has been devoted to the study of the multifractal properties of singular measures. It has been observed that many fractal measures appearing in practice scale differently at different points. Thus if we consider a measure μ on a space X and balls $B_x(\epsilon)$ of radius ϵ centered at x, and define the *singularity strength* of the measure at x by $\alpha(x)$ where

$$\mu(B_x(\epsilon)) \sim \epsilon^{\alpha(x)},$$

then it is frequently observed that $\alpha(x)$ is not constant.

To characterize the size of the sets over which $\alpha(x)$ is constant one may cover the entire support of μ with balls of radius ϵ and let $N_\alpha(\epsilon)$ be the number of balls that scale like ϵ^α for a given value of α. The Hausdorff dimension $f(\alpha)$ of the set on which $\alpha(x) = \alpha$ is then obtained by examining how $N_\alpha(\epsilon)$ scales as $\epsilon \to 0^+$, i.e.,

$$N_\alpha \sim \epsilon^{-f(\alpha)}. \quad (A1)$$

As noted in Ref. 35, instead of a measure μ, we may consider a function F and define the strength of a singularity of F at a point x by

$$|F(B_x(\epsilon))| \sim \epsilon^{\alpha(x)},$$

where $|\cdot|$ is used to denote the size of a set. As discussed in previous sections, $\alpha(x)$ is exactly the Hölder exponent $\gamma(x)$ of the function F at the point x and we may think of $f(\alpha)$ as the Hausdorff dimension $D_H(\gamma)$ of the set of points at which F is Hölder with exponent exactly γ. It follows that the thermodynamic formalism that has been introduced to describe the statistical properties of singular measures, and extended to the case of functions in Ref. 38, can be applied directly to the present problem.[39]

Arneodo *et al.* have introduced a wavelet based method to numerically estimate $D_H(\gamma)$.[35] It can be shown that the wavelet transform

$$W_\Psi[F](b,a) = 1/a \int_{-\infty}^{\infty} \overline{\Psi}((x-b)/a) F(x)\, dx$$

for a wavelet Ψ that is orthogonal to linear functions scales as

$$W_\Psi(x_0, a) \sim a^{h(x_0)}$$

in the limit $a \to 0^+$.[40] (In the preceding, the overbar denotes complex conjugation.) This means that ideally one could determine the Hölder regularity of a function at a point x_0 by computing the exponential decay rate of its wavelet coefficients.

This approach does not circumvent the difficulty posed by the fact that singularities accumulate on each other in the case of fractal functions, and therefore an indirect method needs to be used to approximate quantities like $D_H(\gamma)$. To examine the properties of a function F, we cover its domain with $N(\epsilon)$ balls $B_x(\epsilon)$ and define a *partition function*,

$$\mathcal{Z}(q,\epsilon)=\sum_{i=1}^{N(\epsilon)} |F(B_x(\epsilon))|^q.$$

The function $\mathcal{Z}(q,\epsilon)$ scales as $\epsilon^{\tau(q)}$ as $\epsilon\to 0^+$. A fundamental result in the multifractal formalism states that $\tau(q)$ is the Legendre transform of the singularity spectrum $D_H(\gamma)$ of F. Assuming that τ is differentiable, we can determine $D_H(\gamma)$ from the following relations:

$$D_H(\gamma)=q\gamma-\tau(q),$$

$$\gamma=\frac{d}{dq}\tau(q,j).$$

We briefly mention that since the u coordinates of the iterates of the map defined by Eq. (2) are not distributed uniformly, standard wavelet transform algorithms which rely on tools such as the FFT cannot be used directly. Instead we started with a large number of points, linearly interpolated them, and subsampled the resulting partially linear function on a uniform grid. This procedure tends to smooth out the function at small scales, so care needs to be taken to use only wavelets on scales that are sufficiently large. A similar approach has been used in Ref. 41.

[1] H. Fujisaka and T. Yamada, Prog. Theor. Phys. **69**, 32 (1983); L. M. Pecora and T. L. Carroll, Phys. Rev. Lett. **64**, 821 (1990).

[2] V. Afraimovich, N. N. Verichev, and M. I. Rabinovich, Radiophys. Quantum Electron. **29**, 795 (1986).

[3] M. Rosenblum, A. Pikovsky, and J. Kurths, Phys. Rev. Lett. **76**, 1804 (1996); M. G. Rosenblum, A. S. Pikovsky, and J. Kurths, *ibid.* **78**, 4193 (1997); S. Boccaletti, L. M. Pecora, and A. Pelaez, Phys. Rev. E **63**, 066219 (2001).

[4] F. Varela, J. P. Lachaux, E. Rodriguez, and J. Martinerie, Nat. Rev. Neurosci. **2**, 229 (2001); E. Rodriguez, N. George, J-P. Lachaux, J. Martinerie, B. Renault, and F. J. Varela, Nature (London) **397**, 430 (1999); C. M. Gray, Neuron **24**, 31 (1999).

[5] L. M. Pecora, T. L. Carroll, and J. F. Heagy, Phys. Rev. E **52**, 3420 (1995); H. D. I. Abarbanel, *Analysis of Observed Chaotic Data* (Springer-Verlag, New York, 1996).

[6] S. J. Schiff, P. So, T. Chang, R. E. Burke, and T. Sauer, Phys. Rev. E **54**, 6708 (1996).

[7] N. F. Rulkov, M. M. Sushchik, L. S. Tsimring, and H. D. I. Abarbanel, Phys. Rev. E **51**, 980 (1995).

[8] P. So, E. Barreto, K. Josić, E. Sander, and S. J. Schiff, Phys. Rev. E **65**, 046225 (2002).

[9] The choice of unidirectional coupling is for ease of analysis. With bidirectional coupling, crises may occur and additional dynamical changes might obscure the discussion. However, in certain cases, unidirectionally coupled systems are *locally* equivalent to bidirectionally coupled systems (Ref. 10). Most importantly, we expect the complications (such as wrinkling, cusps, and fractal structures) in the synchronization set discussed here to persist in the bidirectional case.

[10] K. Josić, Phys. Rev. Lett. **80**, 3053 (1998).

[11] The definition of generalized synchrony given in Ref. 7 requires a continuous map between *trajectories* in the phase spaces of the two component systems. Most authors (e.g., Refs. 5, 16, 18) define generalized synchrony via a stronger but more practical condition requiring the existence of a continuous map between *states* of the component phase spaces.

[12] The synchronization set is a graph over X, but attractors for this coupled system may only be subsets of this graph. This is true for both invertible and noninvertible systems.

[13] L. M. Pecora, T. L. Carroll, G. A. Johnson, D. J. Mar, and J. F. Heagy, Chaos **7**, 520 (1997); N. F. Rulkov, *ibid.* **6**, 262 (1996).

[14] H. D. I. Abarbanel, N. F. Rulkov, and M. M. Sushchik, Phys. Rev. E **53**, 4528 (1996).

[15] H. L. Bryant and J. P. Segundo, J. Physiol. (London) **260**, 279 (1976); Z. F. Mainen and T. J. Sejnowski, Science **268**, 1503 (1995).

[16] L. Kocarev and U. Parlitz, Phys. Rev. Lett. **76**, 1816 (1996).

[17] E. Barreto, P. So, B. J. Gluckman, and S. J. Schiff, Phys. Rev. Lett. **84**, 1689 (2000).

[18] B. R. Hunt, E. Ott, and J. A. Yorke, Phys. Rev. E **55**, 4029 (1997).

[19] V. Afraimovich, J.-R. Chazottes, and A. Cordonet, Phys. Lett. A **283**, 109 (2001); K. Josić, Nonlinearity **13**, 1321 (2000); J. Stark, Ergod. Theory Dyn. Syst. **19**, 155 (1999); L. Kocarcv, U. Parlitz, and R. Brown, Phys. Rev. E **61**, 3716 (2000); K. Pyragas, *ibid.* **54**, R4508 (1996).

[20] For a typical point $(\mathbf{x}, \mathbf{y})$ in the synchronization set, consider an orbit segment consisting of the points $\mathbf{F}^{-j}(\mathbf{x},\mathbf{y})$ for $j=1,2,...,T$. The time-T Lyapunov exponents over the orbit segment emanating from $\mathbf{F}^{-T}(\mathbf{x},\mathbf{y})$ can be calculated. If, for $T\to\infty$, this spectrum of Lyapunov exponents remains the same for almost all $(\mathbf{x}, \mathbf{y})$ with respect to the natural measure, then we call these the past-history Lyapunov exponents of the system.

[21] The Hölder exponent of ϕ at x is $\liminf_{\delta\to 0}\{\log|\phi(x+\delta)-\phi(x)|/\log|\delta|\}$ if this quantity is less than 1, and equal to 1 otherwise.

[22] N. Fenichel, Indiana Univ. Math. J. **21**, 193 (1971).

[23] M. W. Hirsch, C. C. Pugh, and M. Shub, *Invariant Manifolds*, Lecture Notes in Mathematics (Springer-Verlag, Berlin, 1977), Vol. 583.

[24] See http://complex.gmu.edu/gallery5.html

[25] C. E. Frouzakis, L. Gardini, I. G. Kevrekidis, G. Millerioux, and C. Mira, Int. J. Bifurcation Chaos Appl. Sci. Eng. **7**, 1167 (1997).

[26] R. M. May, Nature (London) **261**, 459 (1976).

[27] E. Ott, *Chaos in Dynamical Systems* (Cambridge University Press, New York, 1993); E. N. Lorenz, J. Atmos. Sci. **20**, 130 (1963); R. H. Simoyi, A. Wolf, and H. L. Swinney, Phys. Rev. Lett. **49**, 245 (1982); W. L. Ditto, S. N. Rauseo, and M. L. Spano, *ibid.* **65**, 3211 (1990); M. R. Guevara, L. Glass, and A. Shrier, Science **214**, 1350 (1981); G. Matsumoto, K. Aihara, M. Ichikawa, and A. Tasaki, J. Theor. Neurobiol. **3**, 1 (1984).

[28] H. Steinlein and H.-O. Walther, J. Dyn. Diff. Eqs. **2**, 325 (1990).

[29] This is similar to the classification of the invariant set within a dynamical horseshoe (see Ref. 30).

[30] K. T. Alligood, T. D. Sauer, and J. A. Yorke, *Chaos: An Introduction to Dynamical Systems* (Springer-Verlag, New York, 1997).

[31] J. C. Chubb, E. Barreto, P. So, and B. J. Gluckman, Int. J. Bifurcation Chaos Appl. Sci Eng. **11**, 2705 (2001).

[32] Reference 33 describes a 1:2 multivalued state that results from a bifurcation of the response system as the coupling is decreased. This is fundamentally different from the mechanism described in the present work, which is based on the intrinsic noninvertibility of the drive. One should note that the examples in Ref. 33 are not *globally* asymptotically stable. This means that for a given history of the drive, two different initial response states do not necessarily have the same asymptotic state on the m branches ($m=2$ in this case). In contrast, the situation considered here is more coherent in the sense that for a given history of the drive, there is only one unique asymptotic response state despite the Cantor-type structure of the synchronization set.

[33] N. F. Rulkov *et al.*, Phys. Rev. E **64**, 016217 (2001); N. F. Rulkov and C. T. Lewis, *ibid.* **63**, 065204 (2001).

[34] M. Barge and W. T. Ingram, Top. Appl. Phys. **72**, 159 (1996).

[35] A. Arneodo, E. Bacry, and J. F. Muzy, *Wavelets in Physics* (Cambridge University Press, Cambridge, 1999).

[36] S. G. Mallat, *A Wavelet Tour of Signal Processing*, 2nd ed. (Academic, New York, 1999).

[37] C. J. Morales and E. Kolaczyk, Anal. Biomed. Eng. **30**, 588 (2002).

[38] S. Jaffard, SIAM (Soc. Ind. Appl. Math.) J. Math. Anal. **28**, 944 (1997); **28**, 971 (1997).

[39] See, for example, C. Beck and F. Schlögl, *Thermodynamics of Chaotic Systems* (Cambridge University Press, Cambridge, 1993).

[40] Since in this paper we are only interested in the Hölder exponent we only require Ψ to be orthogonal to first degree polynomials. If the synchronization manifold is differentiable, the regularity of its higher derivatives can be studied using wavelets orthogonal to higher order polynomials (Ref. 35).

[41] R. de la Llave and N. Petrov, Exp. Math. (in press).